Competition between biogeochemical drivers and land-cover changes determines urban greening or browning

Long Li [a], Wenfeng Zhan [a, b, *], Weimin Ju [a], Josep Peñuelas [c, d], Zaichun Zhu [e], Shushi Peng [f], Xiaolin Zhu [g], Zihan Liu [a], Yuyu Zhou [h], Jiufeng Li [a], Jiameng Lai [a], Fan Huang [a], Gaofei Yin [i], Yongshuo Fu [j], Manchun Li [b,k], Chao Yu [l]

a Jiangsu Provincial Key Laboratory of Geographic Information Science and Technology, International Institute for Earth System Science, Nanjing University, Nanjing,

Jiangsu, China

b Jiangsu Center for Collaborative Innovation in Geographical Information Resource Development and Application, Nanjing, China

c CSIC, Global Ecology Unit CREAF-CSIC-UAB-UB Bellaterra, Barcelona, Catalonia, Spain

d CREAF, Bellaterra, Barcelona, Catalonia, Spain

e Peking University Shenzhen Graduate School, Peking University, Shenzhen, Guangdong, China

f Sino-French Institute for Earth System Science, College of Urban and Environmental Sciences, Peking University, Beijing, China

g Department of Land Surveying and Geo-Informatics, The Hong Kong Polytechnic University, Hong Kong, China

h Department of Geological and Atmospheric Sciences, Iowa State University, Ames, IA, USA

[i] *Faculty of Geosciences and Environmental Engineering, Southwest Jiaotong University, Chengdu, China*

[j] *College of Water Sciences, Beijing Normal University, Beijing, China*

[k] *School of Geography and Ocean Science, Nanjing University, Nanjing, China*

[l] *State Key Laboratory of Remote Sensing Science, The Aerospace Information Research Institute, Chinese Academy of Sciences, Beijing, China*

CONTACT INFORMATION

*** Corresponding author:** W. Zhan (zhanwenfeng@nju.edu.cn).

1. *CSIC, Global Ecology Unit CREAF-CSIC-UAB-UB Bellaterra, Barcelona 08193, Catalonia, Spain*

2. *CREAF, Bellaterra, Barcelona 08193, Catalonia, Spain*

ABSTRACT

Urban vegetation, a harbinger of future global vegetation change, is controlled by complex urban environments. The urban-rural gradient in vegetation greenness trends and their responses to biogeochemical drivers (e.g. elevated atmospheric CO2 concentration and climate warming) and land-cover changes, however, remain unclear. Here we used satellite-derived enhanced vegetation index to examine the greenness trends for 1500-plus cities in China for 2000–2019. We developed a conceptual framework to differentiate between the contributions of four key drivers to the greenness trends: two biogeochemical drivers, a background biogeochemical driver (BBD) and an urban biogeochemical driver (UBD), and two drivers of land-cover changes, urban expansion or densification (UED) and urban green recovery (UGR). We find that the greening trends gradually decreased from urban cores to urban new towns and then to browning trends in urban fringes. The significant greening in urban cores was mainly contributed by BBD (25.6%) and UBD (52.3%). While the minor greening in urban new towns was contributed by both BBD (33.1%) and UBD (24.1%) and weakened by UED (—39.7%). The UED (—64.4%) dominated the browning in urban fringes. These results suggest that biogeochemical drivers and land-cover changes jointly regulated the urban-rural gradient in greenness trends, which contributes to the assessment of future global vegetation change driven by complex environmental changes.

INTRODUCTION

As a key component of terrestrial ecosystems, vegetation is extremely critical in maintaining carbon cycles and providing ecological services (Lee et al., 2011; Forzieri et al., 2017; Piao et al., 2020). Global-scale studies have reported that the recent greening of the Earth is regulated by a series of biogeochemical drivers (e.g. the effect of atmospheric CO_2 fertilization, nitrogen deposition, and climate change) and land-cover changes (Nemani et al., 2003; Los, 2013; Schimel et al., 2015; Zhu et al., 2016; Chen et al., 2019; Piao et al., 2020). Cities are a coupling system between nature and human beings (Grimm et al., 2008), with more than half of the global population currently living in cities (United Nations, 2018). Vegetation in cities differs from natural landscapes and can either be greening or browning, because cities undergo more drastic land-cover changes (Liu et al., 2020) and because changes in urban vegetation are affected by more complex biogeochemical drivers (Gregg et al., 2003; Zhao et al., 2016). Urban environmental changes are the ‘harbingers’ of global change (Grimm et al., 2008). Investigating urban greening (or browning) and its associated drivers is therefore valuable for both human settlements and better predictions of vegetation changes in natural landscapes in the future.

The growth of vegetation can usually be enhanced more in cities than rural land due to the significantly larger urban biogeochemical effect (Gregg et al., 2003; Zhao et al., 2016; Dahlhausen et al., 2018; Jia et al., 2018; Ruan et al., 2019) but naturally does not indicate that the greenness trends are greater in urban than rural areas from a decadal perspective. Several recent studies focusing on decadal changes in urban vegetation have suggested that vegetation could be either greening or browning under various socioeconomic and climatic controls (Du et al., 2019; Corbane et al., 2020;

Liang et al., 2020). Two important issues, however, persist. First, urban environmental change depends strongly on the background climate (Zhao et al., 2014) and city size (Oke, 1973), and trends of urban vegetation greenness are anticipated to be highly spatially heterogeneous along the urban-rural gradient. The urban-rural gradient in the trends of vegetation greenness nevertheless remains poorly known, especially its dependence on background climate and city size. Second, the recent greening of natural vegetation is mainly regulated by biogeochemical drivers (Zhu et al., 2016; Piao et al., 2020), but urbanization is usually accompanied by significantly more complex land-cover changes such as urban expansion (or densification) and renewal (Seto et al., 2012; Zheng et al., 2014). How the trends of the urban-rural gradient of greenness is affected by the combination of biogeochemical drivers and land-cover changes, therefore, remains unclear.

Facing these challenges, we investigated the greenness trends identified by satellite-derived data for the enhanced vegetation index (EVI) and the associated biogeochemical drivers and land-cover change for >1500 cities in China for 2000-2019. China has undergone extremely rapid urbanization in the last two decades and is an ideal laboratory for investigating trends of vegetation greenness in response to both global and urban environmental change. We divided the developed areas of a city into three categories, urban cores, urban new towns, and urban fringes, and divided the rural background of a city into two categories, rural fringes and rural backgrounds (Supplementary Fig. 1). We further examined the greenness trend of each city category under different city sizes and background climates. We propose a 'reference' method to differentiate between the contributions of biogeochemical drivers (urban and background biogeochemical drivers) and land-cover changes (urban expansion or densification and green recovery) to the greenness trend. This study should help to deepen our understanding of future changes to vegetation under global climate change.

RESULTS AND DISCUSSION

Greenness trends in urban surfaces and their surroundings

The variations in greenness trends from urban cores to rural backgrounds were typically V-shaped (a decrease followed by an increase) (Fig. 1). Greenness trends gradually decreased from urban cores to urban fringes and shifted from greening (for urban cores and urban new towns) to browning (urban fringes), but browning again shifted to greening from urban fringes to rural backgrounds. Greenness trends in urban cores were as large as 0.014 ± 0.015 decade^{-1} (mean ± 1 SD), with 75% of the cities having a greening trend (Fig. 1a). Greenness trends in urban new towns were only 0.006 ± 0.020 decade^{-1}, with similar proportions of cities having greening (53%) and browning trends (47%). More cities had a greening trend in northern than southern China (Fig. 1b). The mean greenness trend in urban fringes became negative (−0.015 ± 0.023 decade^{-1}), and only 27% of the cities had a greening trend, again mainly distributed in northern China (Fig. 1c). The mean greenness trend in rural fringes became positive again (0.026 ± 0.016 decade^{-1}). Only 16% of the cities in this category had a browning trend, mostly in southwestern and eastern China (Fig. 1d). The rural backgrounds of almost all cities (99%) had significant greening trends (0.033 ± 0.013 decade^{-1}), with only a few exceptions (Fig. 1e).

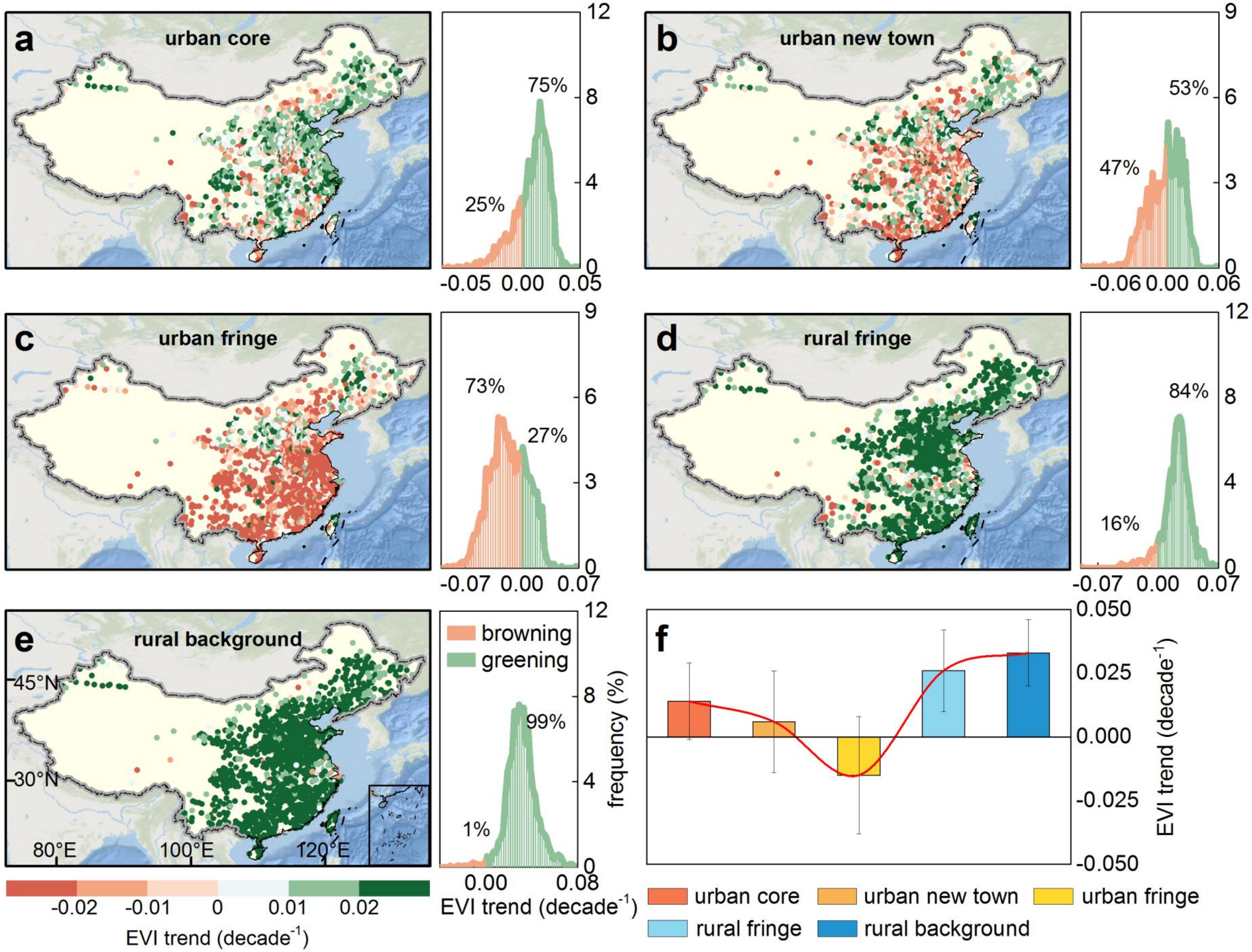
a
urban core
75%
25%
b
urban new town
53%
47%
c
urban fringe
73%
27%
d
rural fringe
84%
16%
e
rural background
45°N
30°N
80°E
100°E
120°E
browning
greening
99%
1%
frequency (%)
EVI trend (decade-1)
f
EVI trend (decade-1)
urban core
urban new town
urban fringe
rural fringe
rural background

137

Fig. 1. Annual mean EVI trends of the urban and rural categories for >1500 cities in China | Mean EVI trends for urban cores (**a**), urban new towns (**b**), urban fringes (**c**), rural fringes (**d**), and rural backgrounds (**e**), and comparisons among these five categories (**f**). This analysis is based on pixels with significant EVI changes at $P < 0.05$. The percentage of pixels with significant changes for each city is given in Supplementary Fig. 2.

The greenness trends all increased with city size for the three urban categories but not for the two rural categories (Fig. 2a). The EVI trend for urban cores increased from 0.004 ± 0.016 decade^{-1} for small towns to 0.019 ± 0.012 decade^{-1} for megacities. The EVI trend for urban new towns increased with city size from −0.003 ± 0.022 to 0.009 ± 0.017 decade^{-1}, indicating a gradual shift from browning (for small towns, small cities, and medium-sized cities) to greening (for large cities and megacities. The EVI trend for urban fringes increased from −0.021 ± 0.024 to −0.013 ± 0.024 decade^{-1}, demonstrating a gradually decreasing browning trend with city size. In contrast, the variations in the EVI trends for both rural fringes and rural backgrounds were not significantly correlated with city size; the differences in the EVI trends among cities with various sizes were small. Such an urban-rural disparity in the relationship between greenness trend and city size was probably due to the considerably greater effect of cities on urban than rural vegetation (Jia et al., 2021; see the next section for a quantitative analysis).

The trends of urban greenness also depended strongly on background climate (Fig. 2b). For cities in the middle/cold temperate zone, all three urban categories had greening trends: the EVI trends were 0.015 ± 0.012 decade^{-1} (urban cores), 0.013 ± 0.015 decade^{-1} (urban new towns), and 0.005 ± 0.017 decade^{-1} (urban fringes). By comparison, these three urban categories all had browning trends for the tropical cities, with EVI trends of −0.003 ± 0.012 decade^{-1} (urban cores), −0.012 ± 0.016 decade^{-1} (urban new towns), and −0.005 ± 0.023 decade^{-1} (urban fringes). For the cities in the vertical temperate, warm temperate, and subtropical zones, urban greening and browning occurred simultaneously for the three urban categories: urban fringes had browning trends, and urban cores and urban new towns had greening trends. The EVI trend variations between the two rural categories were similar across various background climates and were mostly consistent with previous greening analyses that focused on natural vegetation rather than cities (Zhu et al., 2016; Piao et al., 2020).

Further analysis suggested that greening and browning trends could co-exist across the three urban categories even within a single city (Supplementary Fig. 3). Such a co-existence may be one of the reasons for the controversy in urban greening or browning reported by previous studies. For example, cities in the vertical temperate zone were reported to mostly have browning trends (Liang et al., 2020), but other studies reported greening trends (Du et al., 2019; Corbane et al., 2020). Another example is the inconsistent observation of greening or browning for warm temperate and subtropical cities (Du et al., 2019; Corbane et al., 2020; Liang et al., 2020). The percentage of cities in our study with simultaneous greening and browning trends across all three urban categories was highest for the subtropical zone (67%), followed by the vertical temperate zone (64%), the warm temperate zone (50%), the middle/cold temperate zone (45%), and the tropical zone (32%, implying that arriving at contradictory interpretations of urban greening or browning in the first three climatic zones was more likely when the three urban categories were not well delineated. That is, the possible sources of this controversy among previous studies were the different city boundaries used to delineate urban surfaces and the vague or lack of differentiation of the urban categories.

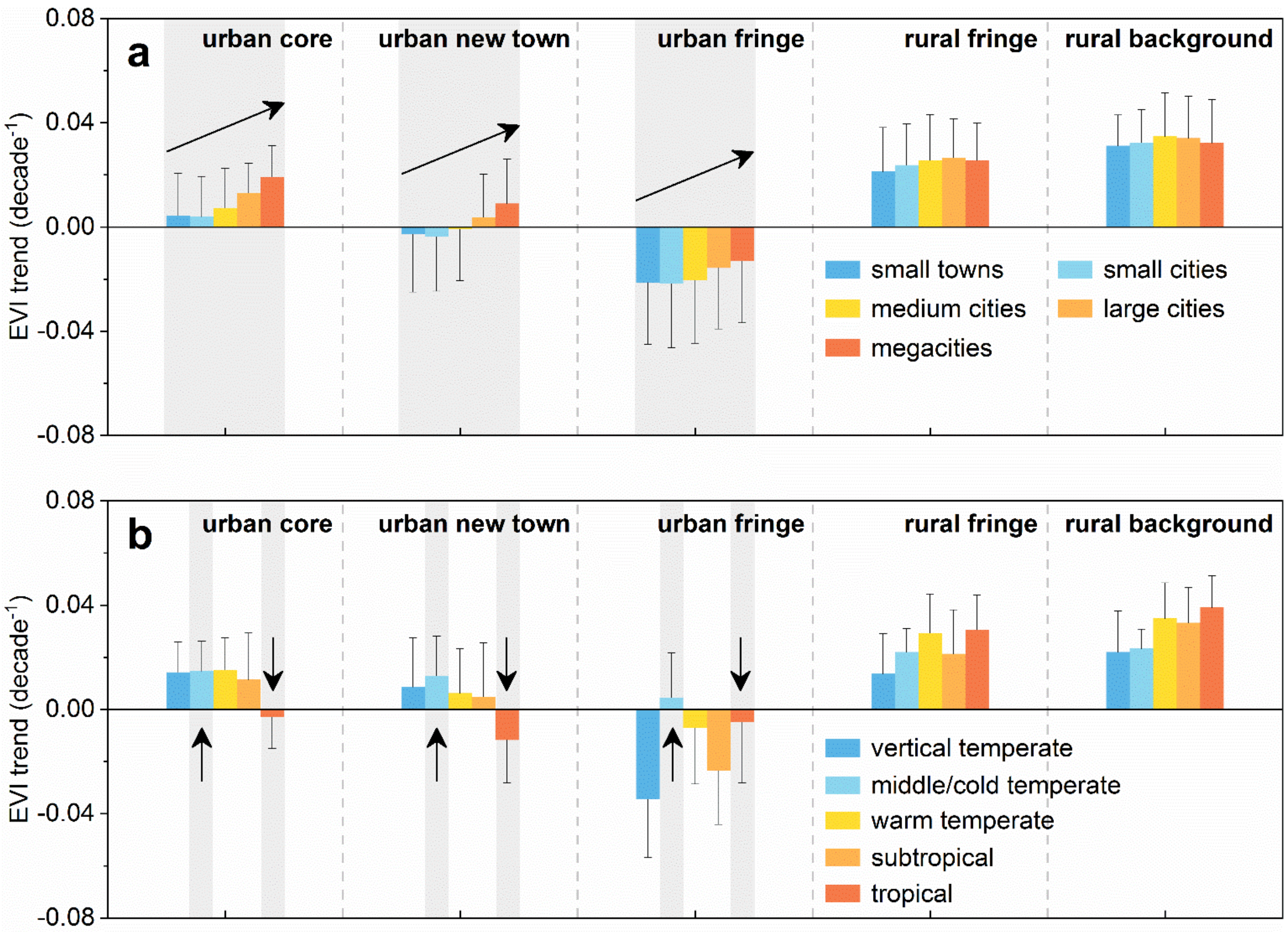

Fig. 2. Variations in annual mean EVI trends in the three urban categories (urban cores, urban new towns, and urban fringes) and the two categories of rural surroundings (rural fringes and rural backgrounds) depending on city size (a) and background climate (b) | The arrows in (**a**) indicate that the EVI trends increase with city size, and the upward and downward arrows in (**b**) indicate the climatic zones in which the three urban

categories have a consistent greening or browning trend, respectively.

Contributions of biogeochemical drivers and land-cover changes to greenness trends

The greenness trends within a city were mainly regulated by the biogeochemical drivers and land-cover changes (Fig. 3). The significant greening in urban cores was mainly regulated by the biogeochemical drivers (77.8%) rather than land-cover changes (16.1%). In contrast, the noteworthy browning of urban fringes was mainly due to land-cover changes (64.4%) rather than biogeochemical drivers (32.6%). The simultaneous greening and browning for urban new towns was controlled by similar contributions of these two types of drivers, although more cities had greening than browning due to the marginally larger contribution from the biogeochemical drivers (57.2%) than land-cover changes (39.8%; Figs. 1 & 3). The synergy of the biogeochemical drivers and land-cover changes can determine greenness trends (Piao et al., 2015; Zhu et al., 2016; Chen et al., 2019), but these studies mainly focused on natural terrestrial ecosystems rather than cities. We also found that these two types of drivers acted as competitors within cities; greening occurred when the biogeochemical drivers dominated, and browning occurred when land-cover changes dominated (e.g. urban expansion or densification) (Fig. 3). These findings differed from the case of natural ecosystems, in which biogeochemical drivers (e.g. fertilization effect of atmospheric CO_2 concentration) (Piao et al., 2015; Zhu et al., 2016) and land-cover changes (e.g. afforestation; Chen et al., 2019) mostly promote greening concurrently.

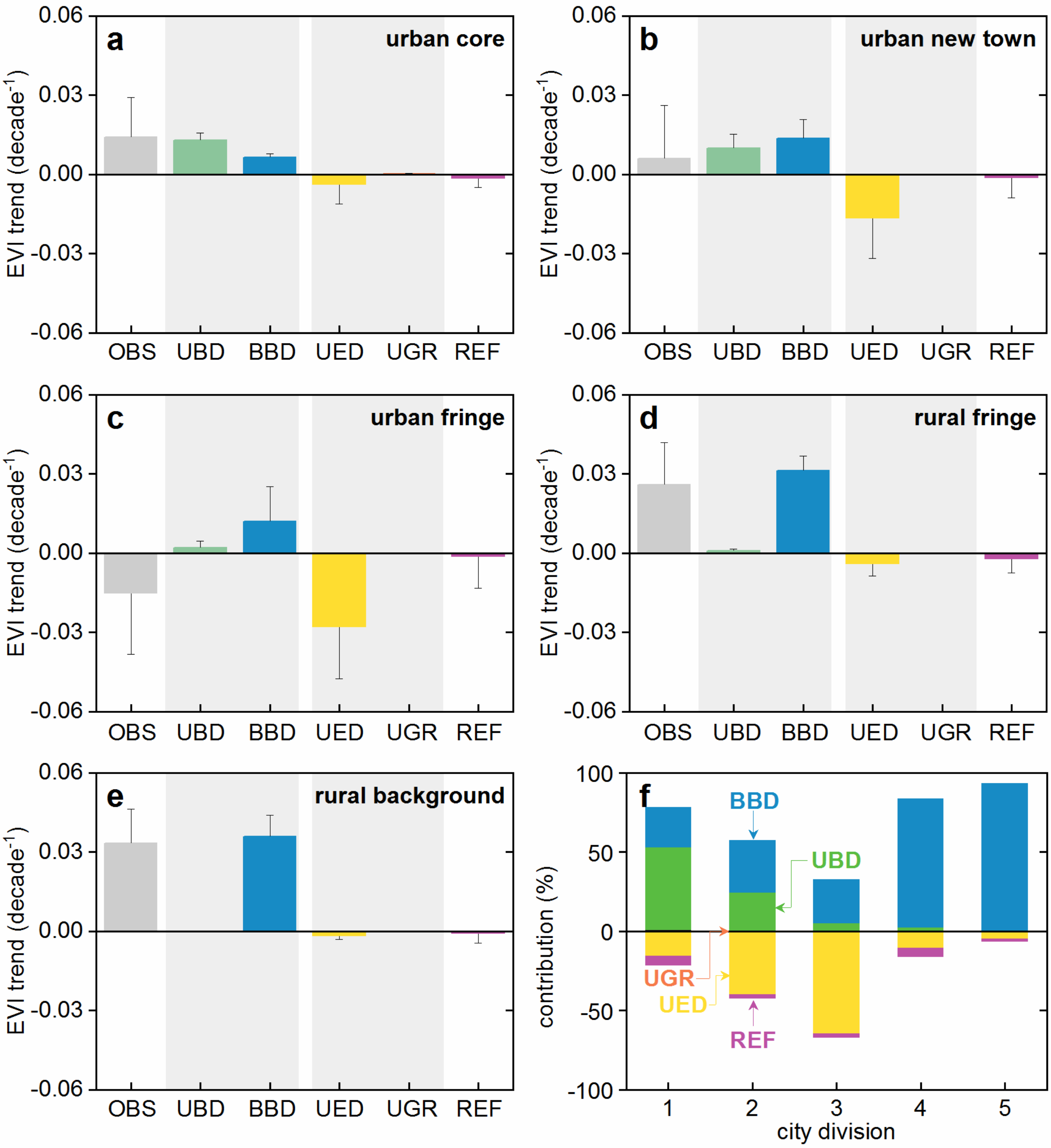

Fig. 3. Contributions (decade^{-1} and percentage) of the background biogeochemical driver (BBD), the urban biogeochemical driver (UBD), urban expansion or densification (UED), urban green recovery (UGR), and a residual factor (REF) to the observed EVI trends (OBS) across the city categories | The two gray rectangles in (**a**) to (**e**) represent the biogeochemical drivers (BBD and UBD) and land-cover changes (UED and UGR), and the numbers 1, 2, 3, 4, and 5 on the x-axis in (**f**) correspond to urban cores, urban new towns, urban fringes, rural fringes, and

rural backgrounds, respectively.

We used two categories of biogeochemical drivers, the background biogeochemical driver (BBD, representing the background controls of surface greening when cities are absent) and the urban biogeochemical driver (UBD, representing the additional factors arising from cities) (Supplementary Fig. 4). We differentiated between the contributions from these two categories of biogeochemical drivers and found that their contributions to the local greenness trends varied with city category. The greening of rural fringes and rural backgrounds was mainly regulated by BBD, with contributions of 81.6 and 93.3%, respectively. For the three urban categories (urban cores, urban new towns, and urban fringes), the contribution of BBD was <30% (Fig. 3). The contribution of UBD was highest in urban cores and gradually decreased along the urban-rural gradient from urban cores to rural backgrounds (the contributions were 52.3, 24.1, 5.0, 2.3, and 0%, respectively; Fig. 3a & f). The contribution of UBD in urban cores could be even larger than that of BBD, but the contributions were the opposite for urban new towns and urban fringes. The enhancement of annual vegetation growth was larger in urban than rural environments due to the urban effect (Gregg et al., 2003; Zhao et al., 2016; Dahlhausen et al., 2018; Jia et al., 2018; Ruan et al., 2019). We also found that urban greening could be significantly enhanced by UBD from a decadal perspective. We provide the first quantitative analysis of the gradual variations in the contributions of UBD and BBD to the trends of surface greenness along the urban-rural gradient.

The drivers of land-cover change could also be divided into two categories, urban expansion or densification (UED, the alteration from natural to impervious surfaces) and urban green recovery (UGR, the transformation from developed to vegetation-dominated surfaces due to urban renewal) (Supplementary Fig. 4). UED and UGR can induce urban browning and greening, respectively. The contribution of UED to the greenness trend decreased from urban cores to urban fringes. UED dominated the browning of urban fringes, with a contribution of -0.028 ± 0.020 decade^{-1} ($-64.4 \pm 46.0\%$) (Fig. 3). Its contribution was lower for urban new towns but remained sufficiently significant (-0.016 ± 0.015 decade^{-1}; $-39.7 \pm 37.2\%$), indicating that continuous urban densification would lead to the significant browning of urban new towns, although this category was already urbanized before 2000 (Supplementary Fig. 1). The contribution of UED was smaller for urban cores (-0.004 ± 0.007 decade^{-1}; $-15.6 \pm 29.6\%$). The contribution of UGR was considerably lower than the contribution of UED. The contribution of UGR among the three urban categories was highest for urban cores, with a value of only 0.00013 ± 0.00017 decade^{-1} ($0.50 \pm 0.70\%$); its contribution was even smaller for the other two urban categories (<0.50%; Fig. 3). Green recovery (e.g. new parks or green spaces) is a major contributor to the greening of urban cores in Chinese cities (Sun et al., 2020), but our results strongly suggested that this factor was negligible. Our findings were consistent with the intra-city land-cover mapping, where pixels of green recovery account for <1% of the total developed surfaces across Chinese cities (Liu et al., 2020).

The increasing trend in greenness with city size for all three urban categories was probably due to the effect of UBD, indicated by the increasing contribution of UBD with city size. For example, the contribution of UBD in urban cores increased from 0.006 ± 0.002 decade^{-1} in small towns to 0.017 ± 0.003 decade^{-1} in megacities (Fig. 4a). Larger cities usually had higher rates of increase of urban atmospheric CO_2

concentrations, urban temperatures, and urban nitrogen deposition (Tian et al., 2020). The combination of the boosted impacts of these biogeochemical factors could therefore lead to a stronger greenness trend in larger cities. The contribution of UED was also larger in larger cities. For example, the negative contribution of UED in urban fringes increased from -0.019 ± 0.021 decade^{-1} in small towns to -0.028 ± 0.020 decade^{-1} in megacities. Such a positive relationship was significant for urban new towns and urban fringes but weaker for urban cores, perhaps due to the more intense urban expansion or densification of larger cities in urban new towns and fringes compared with urban cores (Liu et al., 2020).

The greenness trends in the three urban categories were also affected by background climate (Fig. 4b). The significant greening in the three urban categories in the middle/cold temperate zone was regulated more by the biogeochemical drivers than by land-cover changes. For example, the combination of the BBD and UBD contributions (0.021 decade^{-1}) was larger than the combination of the UED and UGR contributions (-0.016 decade^{-1}), even for urban fringes. In contrast, UED in the tropical zone was the main contributor to the urban browning in the three urban categories (e.g. the UED contribution was -0.029 ± 0.019 decade^{-1} for urban fringes). Such a contrast was probably due to the different major factors restraining urban vegetation growth between these two climatic zones. Surface temperature is the main restraining factor for middle/cold temperate cities at relatively high latitudes (Lucht et al., 2002; Xu et al., 2013), and urban land management is the main restraining factor for tropical cities where the vegetation is dense. The significant increasing rate of urban heat island intensity in temperate cities (Yao et al., 2021), under which the growing season can be prolonged, should be the main regulator of the significant urban greening in this zone.

The faster urbanization in tropical than temperate cities (Song et al., 2020) should contribute to urban browning in the tropics. The greening of urban cores and urban new towns in the vertical temperate, warm temperate, and subtropical zones was mainly regulated by the biogeochemical drivers, and the browning of urban fringes was affected more by urban expansion or densification (Fig. 4b). The greenness trends for the cities in these three zones were comparable, but the contributions of the associated drivers nevertheless differed slightly, especially for subtropical cities. Urbanization has been faster in the tropics, and the effect of urban expansion or densification is more intense than in the vertical temperate and warm temperate zones (Song et al., 2020). The contribution of biogeochemical drivers in subtropical cities, however, was also larger, which neutralized more of the browning induced by UED.

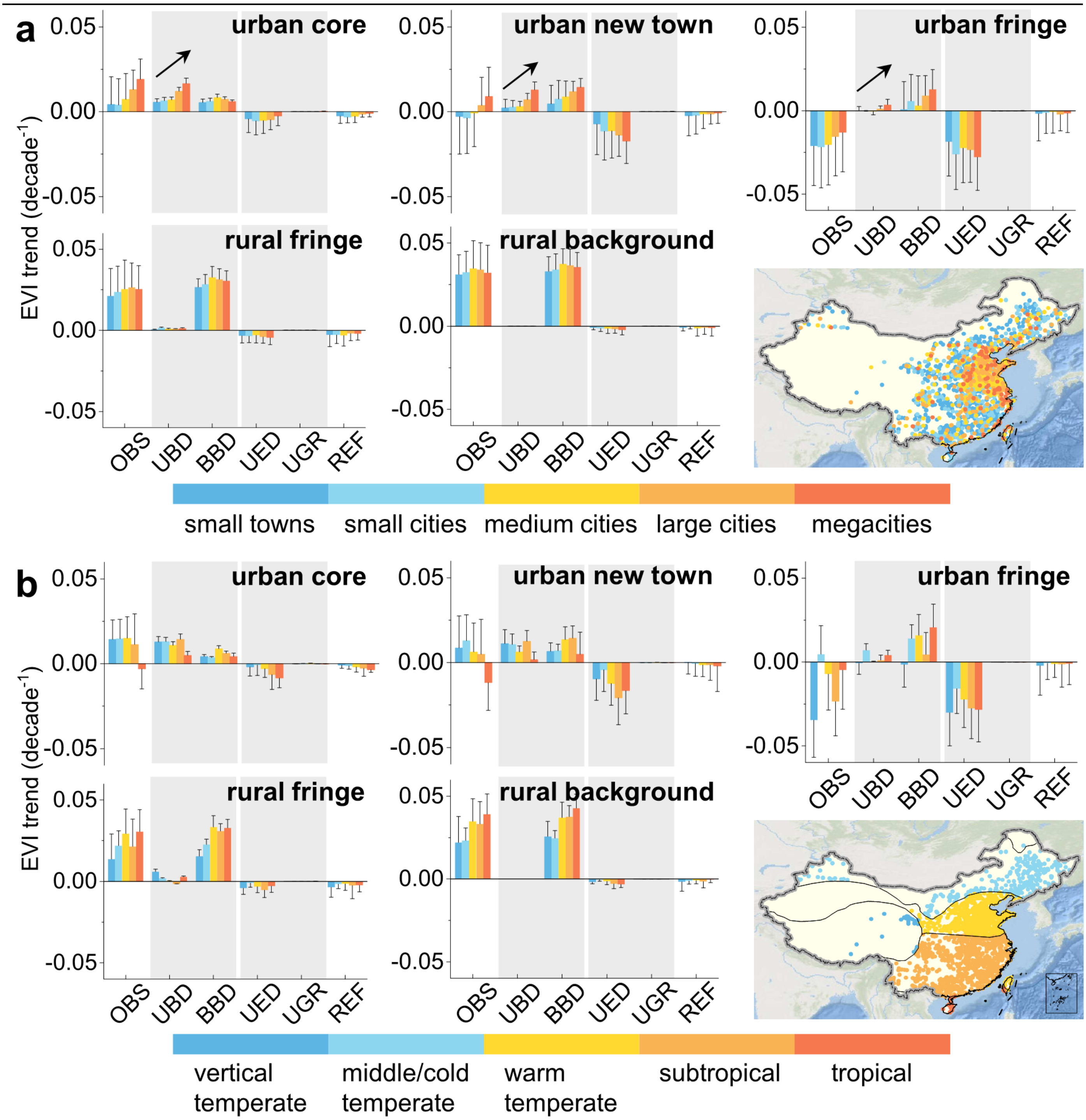

Fig. 4. Contributions (decade^{-1}) of UBD, BBD, UED, UGR, and REF to the observed EVI trends (OBS) depending on city size (a) and background climate (b) | The arrows in (**a**) indicate an increasing UBD contribution with city size, and the two gray rectangles in each plot highlight the contributions of the two biogeochemical drivers (UBD and BBD) and the two drivers of land-cover change (UED and UGR).

Implications

Urban environmental changes are signs of global change. Investigating greenness trends and their associated drivers over many cities is critical for understanding the trends and mechanisms of vegetation changes under future global change. We found that the variations in greenness trends for >1500 Chinese cities were Λ-shaped, from urban cores to rural backgrounds (Fig. 1f). We also found that the biogeochemical drivers and land-cover changes determined this characteristic V-shape to a large extent (Fig. 3). Specifically, urban cores had the largest greening trend among the three urban categories. The urban cores had only 20.3% of the vegetation coverage of the rural backgrounds, but the greenness trend was nevertheless 42.4% of the rural backgrounds, mainly affected by the large contribution of UBD in the urban cores. The greening trends were weaker in urban new towns. The vegetation coverage of this urban category 50.3% of the coverage in rural backgrounds, but its greenness trend was only 18.2% of that in rural backgrounds. Such a weak greening trend in urban new towns was mainly due to the neutralization between the biogeochemical drivers and urban densification. The significant browning for urban fringes could be attributed to the greening induced by the inadequacy of the biogeochemical drivers to compensate the browning caused by urban expansion. The vegetation coverage of urban fringes was 71.2% of that of rural backgrounds, but the greenness trend of urban fringes became negative and was −45.5% of that in rural backgrounds.

The area of urban greening in large cities in China is 32% of that of global cities (Sun et al., 2020). Sun et al. (2020), however, ignored the large number of small cities. We found that the greening trend in China was much larger for large than small cities (Fig. 2), implying that focusing on large cities cannot well lead to a full understanding of the trends of urban greenness. Lager cities are truly the benchmark for urbanization in the future, but the overall quality of future urbanization depends more on the development of the many and widely distributed small cities (or towns) (Fahmi et al., 2014). Regulation of the biogeochemical drivers is relatively difficult, so using urban land management (e.g. urban renewal) as an effective way to narrow the gap of greenness trends between small and large cities is therefore plausible. We also found that browning in tropical cities occurred in all three urban categories (urban cores, urban new towns, and urban fringes) due to urban expansion or densification, despite the high vegetation coverage in these cities. Using urban land management as a critical way to increase the urban green space and sustainability for tropical and/or small cities is therefore urgent.

Our findings indicated that the mean contribution of green recovery to the trends of urban greenness for >1500 cities was relatively small (Fig. 3). These findings, however, do not negate the importance of green recovery to urban greening and urban ecological services. Green recovery can still contribute significantly to urban greening in individual cities using appropriate urban planning. For example, the area of green recovery was 54.7 km^2 in the urban core of Beijing, with its contribution 35.1% of that for all urban cores. With the advance of urbanization, China would face an intensified human-land conflict in per capita green space in the future (Chen et al., 2017). As one of the most direct strategies of urban planning to achieve urban greening (Supplementary Fig. 5), urban green recovery continues to have great potential for enhancing urban ecosystem services.

367

MATERIALS AND METHODS

Study area and materials

Cities in China vary greatly in size and background climate (Jia et al., 2021), and urbanization has been rapid in recent decades (Kuang, 2020). Drastic changes in both biogeochemical cycles and land-cover types for urban surfaces and associated rural surroundings have accompanied the rapid urbanization. Cities in China are therefore ideal laboratories for examining how trends of surface greenness can be simultaneously affected by biogeochemical drivers and land-cover changes. This study focused on all county-level or larger cities in China, a total of 1560 cities. These cities were divided into five categories depending on urban area: 519 small towns (with a mean urban area of 10 km^2), 417 small cities (26 km^2), 312 medium-sized cities (56 km^2), 207 large cities (134 km^2), and 105 megacities (341 km^2) (Supplementary Fig. 6). These cities were in six climatic zones: 29 cities in the vertical temperate zone, 247 cities in the middle/cold temperate zone, 581 cities in the warm temperate zone, 683 cities in the subtropical zone, and 20 cities in the tropical zone.

We used two vegetation indices, the normalized difference vegetation index (NDVI) and the enhanced vegetation index (EVI), both from the MOD13Q1 MODIS product, with a spatial resolution of 250 m and a temporal resolution of 16 d, ranging from March 2000 to February 2020. NDVI can better indicate vegetation coverage and is therefore used to estimate percent vegetation cover (PVC) (Purevdorj et al., 1998). EVI has been extensively used as a proxy of vegetation greenness (Xu et al., 2011; Zhang et al., 2017; Zhou et al., 2014) due to its greater sensitivity to changes in vegetation greenness over surfaces with high biomass (Huete et al., 2002). We also used the yearly MCD12Q1 MODIS data product for land cover and land use with a spatial resolution of 500 m, for the same period. Pixels labeled as water bodies were excluded to eliminate the impact of water bodies on the detection of trends of urban greenness.

We used the urban boundary data for 1990, 2000, and 2018 generated using a globally consistent boundary definition and mapping method (Li et al., 2020). These urban boundary data were applied for categorizing the urban and rural areas. We used the annual data for global artificial impervious area (GAIA) (Gong et al., 2020) to quantify the contribution of urban expansion or densification to the urban-rural gradient in greenness trends. The GAIA data had an overall accuracy of >90% and a spatial resolution of 30 m (Gong et al., 2020). We used the yearly data for urban green recovery (Liu et al., 2020) to quantify the contribution of urban green recovery to the greenness trends. The spatial resolution of the green-recovery data was also 30 m, with an overall accuracy of about 80% (Liu et al., 2020). The GAIA and green-recovery data were both resampled to 250 m to match the spatial resolution of the vegetation indices using majority resampling.

Estimation of urban-rural gradient in greenness trends

The trends of urban greenness are anticipated to be closely associated with city category and indirectly associated with the local status of the biogeochemical drivers and land-cover changes. We divided the urban and rural surfaces of a city into five categories, three urban and two rural: (1) urban cores (delineated by the urban boundaries in 1990), (2) urban new towns (delineated by the urban boundaries between 1990 and 2000), (3) urban fringes (delineated by the urban boundaries between 2000 and 2018, (4) rural fringes (buffer zones surrounding the urban peripheries), and (5) rural backgrounds (buffer zones far from the urban peripheries) (Supplementary Fig. 1). The interannual trends of EVI were then examined for all five city categories using linear regression. Only pixels with statistically significant changes in EVI at $P < 0.05$ were included in the analysis. The category-based pixel percentages with significant EVI changes ($P < 0.05$) are also provided for assessing the representativeness of the significant samples. The greenness trends may also depend on vegetation type, but we did not consider the impact of vegetation type due to the very complex structure and composition of the urban-rural vegetation gradient. This issue is discussed further in Supplementary Note 1.

Decomposition of greenness trends

The trends of vegetation greenness were determined using two types of drivers, biogeochemical drivers (e.g. effect of fertilization by atmospheric CO_2, nitrogen deposition, and climate change) and land-cover changes (e.g. afforestation) (Zhu et al., 2016; Piao et al., 2015; Piao et al., 2020; Chen et al., 2019). Differentiating between the impacts of atmospheric CO_2 concentration, nitrogen deposition, and climate change on greenness trends is extremely difficult at the local scale within a city (Liang et al., 2020; Zhao et al., 2016), so we combined these factors and referred to them as biogeochemical drivers. Cities had two types of biogeochemical drivers, a background biogeochemical driver (BBD) and an urban biogeochemical driver (UBD). BBD represents the environmental changes arising at a large (global or regional) scale, such as elevated atmospheric CO_2 concentrations, increased nitrogen deposition, and climatic warming (Piao et al., 2020), and UBD represents the urban environmental changes arising at a local (city) scale, such as high CO_2 emissions, nitrogen deposition, and urban heat islands (Zhao et al., 2016). The influence of land-cover changes to the trends of vegetation greenness is also twofold. The first category of urban land-cover change is the transition from natural landscapes to impervious surfaces or the further increase in the percentage of impervious surfaces (Shahtahmassebi et al., 2016), i.e. urban expansion or densification (UED). The second category is the transition from developed to vegetation-dominated surfaces, usually due to a series of urban-renewal activities (Haase et al. 2017), i.e. urban green recovery (UGR). UED generally leads to a decrease in urban vegetation (i.e. urban browning; Gong et al., 2020), and UGR generally leads to an increase in urban vegetation (i.e. urban greening) (Liu et al., 2020). The observed EVI trend (OBS, a proxy for the trends of vegetation greenness) can be expressed as:

$$O = B + U + E + G + r \tag{1}$$

where O is the observed EVI trend (i.e. OBS), and B, U, E, G, and r represent the contributions from BBD, UBD, UED, UGR, and a residual factor (REF), respectively. We used REF to express both the estimation error and the possible influence of other controls in addition to these four drivers (see Supplementary Note 1).

The contributions of BBD, UBD, UED, and UGR vary across a city and therefore depend on city category. We categorized the pixels for each city category into four groups: (1) pixels with urban expansion or densification (labeled as Pix_ED pixels), (2) pixels with green recovery (Pix_GR pixels), (3) pixels with unchanged land-cover type but with a positive EVI trend (Pix_PE pixels), and (4) pixels with unchanged land-cover type but with a negative EVI trend (Pix_NE pixels). The first three groups of pixels (Pix_ED, Pix_GR, and Pix_PE pixels) accounted for 95.1% of the total pixels, and the Pix_NE pixels accounted for only 4.9%. To estimate the contributions of these drivers to the Pix_ED and Pix_GR pixels, we further combined the two categories of pixels with unchanged land cover (i.e. Pix_PE and Pix_NE pixels) and designated them as Pix_LCU pixels. Eqs. (8) to (10) provide more explanations.

The greenness trends of these four groups of pixels (the Pix_ED, Pix_GR, Pix_PE, and Pix_NE pixels) can all be affected by BBD and UBD. We disregarded the Pix_NE pixels, however, in the calculations of the contributions of BBD and UBD due to the low pixel percentage (<5%) compared with the other three types of pixels and partly because the Pix_NE pixels should be affected more by other factors (e.g. change in building height) rather than by the biogeochemical drivers (BBD and UBD), because BBD and UBD both enhance greenness trends and lead to positive EVI trends. The contributions of BBD and UBD to the trends of urban greenness can therefore be estimated by:

$$B = B_{\text{Pix\_PE}} + B_{\text{Pix\_ED}} + B_{\text{Pix\_GR}} \tag{2}$$

$$U = U_{\text{Pix\_PE}} + U_{\text{Pix\_ED}} + U_{\text{Pix\_GR}} \tag{3}$$

where $B_{\text{Pix\_PE}}$, $B_{\text{Pix\_ED}}$, $B_{\text{Pix\_GR}}$, $U_{\text{Pix\_PE}}$, $U_{\text{Pix\_ED}}$, and $U_{\text{Pix\_GR}}$ represent the contributions of BBD and UBD for the associated groups of pixels. By comparison, UED can only affect the EVI trends of the Pix_ED pixels with urban expansion or densification, and UGR can only affect the Pix_GR pixels with green recovery. The contributions of UED and UGR to the EVI trend can therefore be estimated by:

$$E = E_{\text{Pix\_ED}} \tag{4}$$

$$G = G_{\text{Pix\_GR}} \tag{5}$$

where $E_{\text{Pix\_ED}}$ and $G_{\text{Pix\_GR}}$ represent the UED and UGR contributions for the Pix_ED and Pix_GR pixels, respectively. According to Eqs. (2) to (5), the estimates of the contributions of BBD, UBD, UED, and UGR can therefore be transformed to calculate eight parameters: $B_{\mathrm{Pix\_PE}}$, $B_{\mathrm{Pix\_ED}}$, $B_{\mathrm{Pix\_GR}}$, $U_{\mathrm{Pix\_PE}}$, $U_{\mathrm{Pix\_ED}}$, $U_{\mathrm{Pix\_GR}}$, $E_{\mathrm{Pix\_ED}}$, and $G_{\mathrm{Pix\_GR}}$ (see Supplementary Fig. 7). These parameters were calculated separately for each city category.

(1) *Calculation of $B_{\mathrm{Pix\_PE}}$ and $U_{\mathrm{Pix\_PE}}$*

$B_{\mathrm{Pix\_PE}}$ refers to the contribution of BBD to the EVI trend of the pixels with unchanged land-cover type but with a positive EVI trend (i.e. the Pix_PE pixels). This parameter is closely associated with the influence of BBD in rural backgrounds and associated vegetation coverages (see Supplementary Fig. 7a for more explanations). $B_{\mathrm{Pix\_PE}}$ can therefore be calculated using the following three components, (*i*) the contribution of BBD to the EVI trend in rural backgrounds, (*ii*) the ratio of PVC between a specific city category and rural backgrounds, and (*iii*) the ratio between the number of Pix_PE pixels and the total number of pixels for a specific city category. For the first component, the contribution of BBD to the EVI trend of the Pix_PE pixels of a specific urban category can be considered equivalent to that of rural backgrounds, mostly because the rural background chosen was relatively far from the urban categories (Supplementary Fig. 1) and would consequently be rarely affected by UBD (Du et al., 2019). That is, the contribution of BBD to the EVI trend of the Pix_PE pixels of a specific urban category can be indirectly measured using the EVI trends of the Pix_PE pixels of rural backgrounds ($EVI_{\mathrm{Pix\_PE\_RB}}$). For the second component, the accurate calculation of $B_{\mathrm{Pix\_PE}}$ requires the consideration of the PVC difference between a specific urban category and a rural background (Supplementary Fig. 8). That is, $B_{\mathrm{Pix\_PE}}$ is not equivalent to $EVI_{\mathrm{Pix\_PE\_RB}}$, because the PVC difference between a specific urban category and a rural background is usually large. For the third component, $B_{\mathrm{Pix\_PE}}$ is also understandably affected by the ratio between the number of

Pix_PE pixels and the total number of pixels for a specific city category. Based on the above analysis, $B_{\mathrm{Pix\_PE}}$ can therefore be calculated by:

$$B_{\mathrm{Pix\_PE}} = EVI_{\mathrm{Pix\_PE\_RB}} \times \textbf{¡Error!} \times \textbf{¡Error!} \tag{6}$$

where $EVI_{\mathrm{Pix\_PE\_RB}}$ represents the mean EVI trend for the same type of Pix_PE pixels in a rural background, $PVC_{\mathrm{Pix\_PE}}$ and $PVC_{\mathrm{Pix\_PE\_RB}}$ represent the PVC of the Pix_PE pixels for a specific urban category and a rural background, respectively, and $A_{\mathrm{Pix\_PE}}$ and A are the number of Pix_PE pixels for a specific urban category and all pixels for this specific urban category, respectively. The calculation of PVC is explained in more detail in Supplementary Note 2.

$U_{\mathrm{Pix\_PE}}$ refers to the influence of UBD on the EVI trends of the Pix_PE pixels. The EVI trends of the Pix_PE pixels would only be affected by BBD and UBD, because land cover does not change for this group of pixels. $U_{\mathrm{Pix\_PE}}$ can therefore be calculated by removing the contribution of BBD from the EVI trends of the Pix_PE pixels ($EVI_{\mathrm{Pix\_PE}}$), given as:

$$U_{\mathrm{Pix\_PE}} = EVI_{\mathrm{Pix\_PE}} \times \textbf{¡Error!} - B_{\mathrm{Pix\_PE}} \tag{7}$$

where $EVI_{\mathrm{Pix\_PE}}$ represents the mean EVI trend of the Pix_PE pixels for a specific urban category.

(2) *Calculation of $B_{\mathrm{Pix\_ED}}$, $U_{\mathrm{Pix\_ED}}$, $B_{\mathrm{Pix\_GR}}$, and $U_{\mathrm{Pix\_GR}}$*

$B_{\mathrm{Pix\_ED}}$ refers to the contribution of BBD to the EVI trend of the pixels with urban expansion or densification (i.e. the Pix_ED pixels). The urbanization levels for the Pix_ED pixels and the pixels with unchanged land-cover type in the same city category (i.e. the Pix_LCU pixels) are relatively similar, so inferring that the contribution ratio between BBD and UBD for these two types of pixels (the Pix_ED and Pix_LCU pixels) in the same city category are also similar is reasonable (Supplementary Fig. 7b). Such a 'proximity-pixel-reference' method has been widely accepted and used (Peng et al., 2014; Li et al., 2015; Hong et al., 2020). B_{Pix_ED} can therefore be calculated indirectly using (*i*) the EVI trend of the Pix_LCU pixels for the same city category (EVI_{Pix_LCU}) and (*ii*) the proportion of the contribution of BBD to the EVI trend for the Pix_PE pixels:

$$B_{Pix\_ED} = EVI_{Pix\_LCU} \times \textbf{¡Error!} \times \textbf{¡Error!} \qquad (8)$$

where EVI_{Pix_LCU} represents the mean EVI trend of the Pix_LCU pixels for a specific city category, B_{Pix_PE} and U_{Pix_PE} can be estimated using Eqs. (6) and (7), respectively, and A_{Pix_ED} denotes the number of Pix_ED pixels for the associated urban category.

U_{Pix_ED} refers to the influence of UBD on the EVI trend of the pixels with urban expansion or densification (i.e. the Pix_ED pixels). U_{Pix_ED} can be similarly calculated indirectly using (*i*) the EVI trend of the Pix_LCU pixels for the same city category (EVI_{Pix_LCU}) and (*ii*) the proportion of the contribution of UBD to the EVI trend for the Pix_PE pixels:

$$U_{Pix\_ED} = EVI_{Pix\_LCU} \times \textbf{¡Error!} \times \textbf{¡Error!} \qquad (9)$$

Similar to the calculation of B_{Pix_ED} and U_{Pix_ED}, we calculated the contributions of BBD and UBD to the EVI trends for the pixels with green recovery, i.e. B_{Pix_GR} and U_{Pix_GR}. More details on the calculation of these two components are provided in Supplementary Note 3.

(3) *Calculation of E_{Pix_ED} and G_{Pix_GR}*

E_{Pix_ED} refers to the contribution of UED to the EVI trend of the pixels with urban expansion or densification (i.e. the Pix_ED pixels). For the same city category, the only difference in the controls of the trends of surface greenness between the pixels with urban expansion or densification (i.e. the Pix_ED pixels) and the Pix_LCU pixels are due to the contribution of UED. Calculating $E_{\mathrm{Pix\_ED}}$ using the difference of the EVI trends between the Pix_ED and Pix_LCU pixels (Supplementary Fig. 7b) is therefore plausible:

$$E_{\mathrm{Pix\_ED}} = (EVI_{\mathrm{Pix\_ED}} - EVI_{\mathrm{Pix\_LCU}}) \times \textbf{¡Error!} \tag{10}$$

where $EVI_{\mathrm{Pix\_ED}}$ represents the mean EVI trend of the Pix_ED pixels for a specific city category.

$G_{\mathrm{Pix\_GR}}$ refers to the contribution of UGR to the EVI trend of the pixels with green recovery (i.e. the Pix_GR pixels). The calculation of $G_{\mathrm{Pix\_GR}}$ is similar to that of $E_{\mathrm{Pix\_ED}}$; more details are provided in Supplementary Note 3.

We used the methods described above to quantify the contributions of BBD, UBD, UED, and UGR to the EVI trends using Eqs. (2) to (5) for each city category. For a better comparison among the various drivers, we further calculated the percentage contributions of these four drivers based on the procedures described in Supplementary Note 4.

References

Chen, B. et al. Quantitative estimation of 21st-century urban greenspace changes in Chinese populous cities. *Sci. Total Environ.* **609**, 956–965 (2017).

Chen, C. et al. China and India lead in greening of the world through land-use management. *Nat. Sustain.* **2**, 122–129 (2019).

Corbane, C. et al. The grey-green divide: multi-temporal analysis of greenness across 10,000 urban centres derived from the Global Human Settlement Layer (GHSL). *Int. J. Digit. Earth* **13**, 101–118 (2020).

Dahlhausen, J. et al. Urban climate modifies tree growth in Berlin. *Int. J. Biometeorol.* **62**, 795–808 (2018).

Du, J. et al. Effects of rapid urbanization on vegetation cover in the metropolises of China over the last four decades. *Ecol. Indic.* **107**, 105458 (2019).

Fahmi, F. Z. et al. Extended urbanization in small and medium-sized cities: The case of Cirebon, Indonesia. *Habitat Int.* **42**, 1–10 (2014).

Forzieri, G. et al. Satellites reveal contrasting responses of regional climate to the widespread greening of Earth. *Science* **356**, 1180–1184 (2017).

Gong, P. et al. Annual maps of global artificial impervious area (GAIA) between 1985 and 2018. *Remote Sens. Environ.* **236**, 111510 (2020).

Gregg, J. W. et al. Urbanization effects on tree growth in the vicinity of New York City. *Nature* **424**, 183–187 (2003).

Grimm, N. B. et al. Global change and the ecology of cities. *Science* **319**, 756–760 (2008).

Haase, D. Greening cities–To be socially inclusive? About the alleged paradox of society and ecology in cities. *Habitat Int.* **64**, 41–48 (2017).

Hong, S. et al. Divergent responses of soil organic carbon to afforestation. *Nat.*

Sustain. **3**, 694–700 (2020).

Huete, A. et al. Overview of the radiometric and biophysical performance of the MODIS vegetation indices. *Remote Sens. Environ.* **83**, 195–213 (2002).

Jia, W. et al. Vegetation growth enhancement in urban environments of the Conterminous United States. *Glob. Change Biol.* **24**, 4084–4094 (2018).

Jia, W. et al. Urbanization imprint on land surface phenology: The urban–rural gradient analysis for Chinese cities. *Glob. Change Biol.* **27**, 2895–2904 (2021).

Kuang, W. 70 years of urban expansion across China: trajectory, pattern, and national policies. *Sci. Bulletin* **65**, 1970–1974 (2020).

Liang, Z. et al. Exploring the Combined Effect of Urbanization and Climate Variability on Urban Vegetation: A Multi-Perspective Study Based on More than 3000 Cities in China. *Remote Sens-Basel* **12**, 1328 (2020).

Lee, X. et al. Observed increase in local cooling effect of deforestation at higher latitudes. *Nature* **479**, 384–387 (2011).

Liu, X. et al. High-spatiotemporal-resolution mapping of global urban change from 1985 to 2015. *Nat Sustain.* **3**, 564–570 (2020).

Li, X. et al. Mapping global urban boundaries from the global artificial impervious area (GAIA) data. *Environ. Res. Lett.* **15**, 094044 (2020).

Li, Y. et al. Local cooling and warming effects of forests based on satellite observations. *Nat. Commun.* **6**, 1–8 (2015).

Los, S. O. Analysis of trends in fused AVHRR and MODIS NDVI data for 1982–2006: Indication for a CO2 fertilization effect in global vegetation. *Global Biogeochem. Cy.* **27**, 318–330 (2013).

Lucht, W. et al. Climatic control of the high-latitude vegetation greening trend and Pinatubo effect. *Science* **296**, 1687–1689 (2002).

Nemani, R. R. et al. Climate-driven increases in global terrestrial net primary production from 1982 to 1999. *Science* **300**, 1560–1563 (2003).

Oke, T. R. City size and the urban heat island. *Atmos. Environ.* **7**, 769–779 (1973).

Peng, S. S. et al. Afforestation in China cools local land surface temperature. *Proc. Natl. Acad. Sci. USA* **111**, 2915–2919 (2014).

Piao, S. et al. Characteristics, drivers and feedbacks of global greening. *Nat. Rev. Earth Environ.* **1**, 1–14 (2020).

Piao, S. et al. Detection and attribution of vegetation greening trend in China over the last 30 years. *Glob. Change Biol.* **21**, 1601–1609 (2015).

Purevdorj, T. S. et al. Relationships between percent vegetation cover and vegetation indices. *Int. J. Remote Sens.* **19**, 3519–3535 (1998).

Ruan, Y. et al. Enhanced vegetation growth in the urban environment across 32 cities in the Northern Hemisphere. *J. Geophys. Res. Biogeo.* **124**, 3831–3846 (2019).

Schimel, D. et al. Effect of increasing CO2 on the terrestrial carbon cycle. *Proc. Natl Acad. Sci. USA* **112**, 436–441 (2015).

Seto, K. C. Global forecasts of urban expansion to 2030 and direct impacts on biodiversity and carbon pools. *Proc. Natl Acad. Sci. USA* **109**, 16083–16088 (2012).

Shahtahmassebi, A. R. et al. Remote sensing of impervious surface growth: A framework for quantifying urban expansion and re-densification mechanisms. *Int. J. Appl. Earth Obs.* **46**, 94–112 (2016).

Song, Y. et al. How does urban expansion impact people's exposure to green environments? A comparative study of 290 Chinese cities. *J. Clean. Prod.* **246**, 119018 (2020).

Sun, L. et al. Dramatic uneven urbanization of large cities throughout the world in

recent decades. *Nat. Commun.* **11**, 1–9 (2020).
Tian, J. et al. Investigating the urban-induced microclimate effects on winter wheat spring phenology using Sentinel-2 time series. *Agr. Forest Meteorol.* **294**, 108153 (2020).
United Nations. World Urbanization Prospects: The 2018 Revision online edn (2018).
Xu, L. et al. Temperature and vegetation seasonality diminishment over northern lands. *Nat. Clim. Change* **3**, 581–586 (2013).
Xu, L. et al. Widespread decline in greenness of Amazonian vegetation due to the 2010 drought. *Geophys. Res. Lett.* **38**, L07402 (2011).
Yao, R. et al. Long-term trends of surface and canopy layer urban heat island intensity in 272 cities in the mainland of China. *Sci. Total Environ.* **772**, 145607 (2021).
Zhang, Y. et al. Reanalysis of global terrestrial vegetation trends from MODIS products: Browning or greening? *Remote Sens. Environ.* **191**, 145–155 (2017).
Zhao, L. et al. Strong contributions of local background climate to urban heat islands. *Nature* **511**, 216–219 (2014).
Zhao, S. et al. Prevalent vegetation growth enhancement in urban environment. *Proc. Natl Acad. Sci. USA* **113**, 6313–6318 (2016).
Zheng, H. W. et al. A review of recent studies on sustainable urban renewal. *Habitat Int.* **41**, 272–279 (2014).
Zhou, L. et al. Widespread decline of Congo rainforest greenness in the past decade. *Nature* **509**, 86–90 (2014).
Zhu, Z. et al. Greening of the Earth and its drivers. *Nat. Clim. Change* **6**, 791–795 (2016).

Supplementary Information (SI)

This file includes:

A. Supplementary notes

Supplementary Notes 1 to 4

B. Supplementary figures

Supplementary Figures 1 to 8

C. Supplementary references

Supplementary References 1 to 11

A. Supplementary notes

<u>Note 1</u>: *Uncertainties of urban-rural gradients in greenness trends due to drivers other than the biogeochemical drivers and land-cover changes*

In addition to the biogeochemical drivers and land-cover changes, the urban-rural gradient in the satellite-derived greenness trends can also be affected by other drivers such as increases in building height (Zhang et al., 2015), a higher frequency of heat waves (Qiu et al., 2020), and insect-induced disturbance (Tai et al., 2019). Increases in building height during urbanization usually decreases the satellite-derived EVI due to the greater effect of shadows with higher buildings (Zhang et al., 2015). A higher frequency of heat waves and insect-induced disturbance can also interrupt vegetation metabolism, damage vegetation physiological function, and accordingly affect the observed EVI (Qiu et al., 2020; Tai et al., 2019). Vegetation greenness usually increases or remains relatively stable for pixels with a stable land-cover type (Zhu et al., 2016; Piao et al., 2020), so we inferred that the browning of the pixels with unchanged land-cover type (the Pix_NE pixels, see Materials and methods) should be due more to these additional drivers, such as increases in building height. We did not discern the contributions from these additional drivers but incorporated them into the residual term in Eq. (1), mostly because (1) the Pix_NE pixels accounted for <5% of the total pixels and because (2) accurately quantifying the contributions of these additional drivers to the urban-rural gradient in greenness trends currently remains a great challenge and may even be impossible.

The urban-rural greenness trends were also closely associated with vegetation type. We acknowledge that differentiating between types of vegetation cover can help to interpret the urban-rural gradient in greenness trends in response to human activities (e.g. field management) and global change (Piao et al., 2003). Differentiating between the types of urban vegetation across >1500 cities, however, is very difficult and even unfeasible for urban surfaces due to the very complex structure and composition of the vegetation. The vegetation types for rural fringes and rural backgrounds were mainly forest, grassland, and farmland: forests were mainly around the northeastern and southwestern cities, grassland was mainly around the northwestern cities, and farmland was mainly around the eastern cities on plains or in basins. These distributions indicated that standardizing the vegetation types in rural fringes and rural backgrounds was not plausible for all cities, because the type of rural vegetation differed greatly across the background climates. Our study therefore did not examine the impact of vegetation type on the quantification of contribution. Our study is consistent with previous studies of urban-rural contrasts in surface phenology (Zhao et al., 2016; Jia et al., 2018; Tian et al., 2020), for which vegetation type was usually not considered due to the great complexity of vegetation type and structure along the urban-rural gradient.

Note 2: ***Estimation of percent vegetation cover***

The percent vegetation cover (PVC) required for differentiating between the contributions from the background and urban biogeochemical drivers was calculated using linear regression based on NDVI data (Purevdorj et al., 1998; Gao et al., 2020). The MODIS NDVI data during the growing season (April-October) were used, and the thresholds required for this method were set at 0.15 and 0.80, representing the scenarios of no vegetation and full vegetation coverage, respectively (Purevdorj et al., 1998). We acknowledge that uncertainties may occur for the selection of appropriate thresholds for different vegetation types. We nevertheless used a consistent standard of threshold, because this analysis was based on the average PVC of the urban and rural surfaces and because we only used the ratio between the urban and rural PVCs.

Note 3: ***Calculation of $B_{\mathrm{Pix\_GR}}$, $U_{\mathrm{Pix\_GR}}$, and $G_{\mathrm{Pix\_GR}}$***

$B_{\mathrm{Pix\_GR}}$ refers to the contribution of BBD to the EVI trend of the pixels with green recovery (i.e. the Pix_GR pixels). The urbanization level was similar for the Pix_GR and Pix_LCU pixels in the same city category, so deducing that the contribution ratio between BBD and UBD for these two types of pixels in the same city category were also similar was rational (Supplementary Fig. 7b). $B_{\mathrm{Pix\_GR}}$ can therefore be calculated indirectly using (*i*) the EVI trend of the Pix_LCU pixels in the same city category ($EVI_{\mathrm{Pix\_LCU}}$) and (*ii*) the proportion of the contribution of BBD to the EVI trend for the Pix_GR pixels:

$$B_{\mathrm{Pix\_GR}} = EVI_{\mathrm{Pix\_LCU}} \times \text{¡Error!} \times \text{¡Error!} \qquad \text{(S1)}$$

where $EVI_{\mathrm{Pix\_LCU}}$ represents the mean EVI trend of the Pix_LCU pixels for a specific city category, $B_{\mathrm{Pix\_PE}}$ and $U_{\mathrm{Pix\_PE}}$ are obtainable using Eqs. (6) and (7), $A_{\mathrm{Pix\_GR}}$ represents the number of Pix_GR pixels for the associated urban category, and A represents all pixels for this urban category.

$U_{\mathrm{Pix\_GR}}$ refers to the influence of UBD on the EVI trend of the pixels with green recovery (i.e. the Pix_GR pixels). $U_{\mathrm{Pix\_GR}}$ can similarly be indirectly estimated using (*i*) the EVI trend of the Pix_LCU pixels in the same city category ($EVI_{\mathrm{Pix\_LCU}}$) and (*ii*) the proportion of the contribution of UBD to the EVI trend for the Pix_GR pixels:

$$U_{\mathrm{Pix\_GR}} = EVI_{\mathrm{Pix\_LCU}} \times \text{¡Error!} \times \text{¡Error!} \qquad \text{(S2)}$$

$G_{\mathrm{Pix\_GR}}$ refers to the contribution of UGR to the EVI trend of the pixels with green recovery (i.e. the Pix_GR pixels). The contribution of UGR was the only difference in the controls of the trends of surface greenness between the pixels with green recovery (i.e. the Pix_GR pixels) and the Pix_LCU pixels for the same city category.

Calculating $G_{\mathrm{Pix\_GR}}$ using the difference of the EVI trends between the Pix_GR and Pix_LCU pixels was consequently feasible (Supplementary Fig. 7b), given by:

$$G_{\mathrm{Pix\_GR}} = (EVI_{\mathrm{Pix\_GR}} - EVI_{\mathrm{Pix\_LCU}}) \times \textbf{¡Error!} \quad \text{(S3)}$$

where $EVI_{\mathrm{Pix\_GR}}$ represents the mean EVI trend of the Pix_GR pixels for a specific city category.

Note 4: ***Calculation of percent contribution of each driver***

The percent contribution of each driver was calculated by (Liu et al., 2019):

$$C_i = \textbf{¡Error!} \times 100\% \quad \text{(S4)}$$

where C_i represents the percent contribution of driver i to the EVI trend ($i = B$, U, E, G, or r). We used the absolute instead of the original values to calculate the contributions to avoid the percent contribution of a single factor >100% and to avoid a denominator equal to zero.

B. Supplementary figures

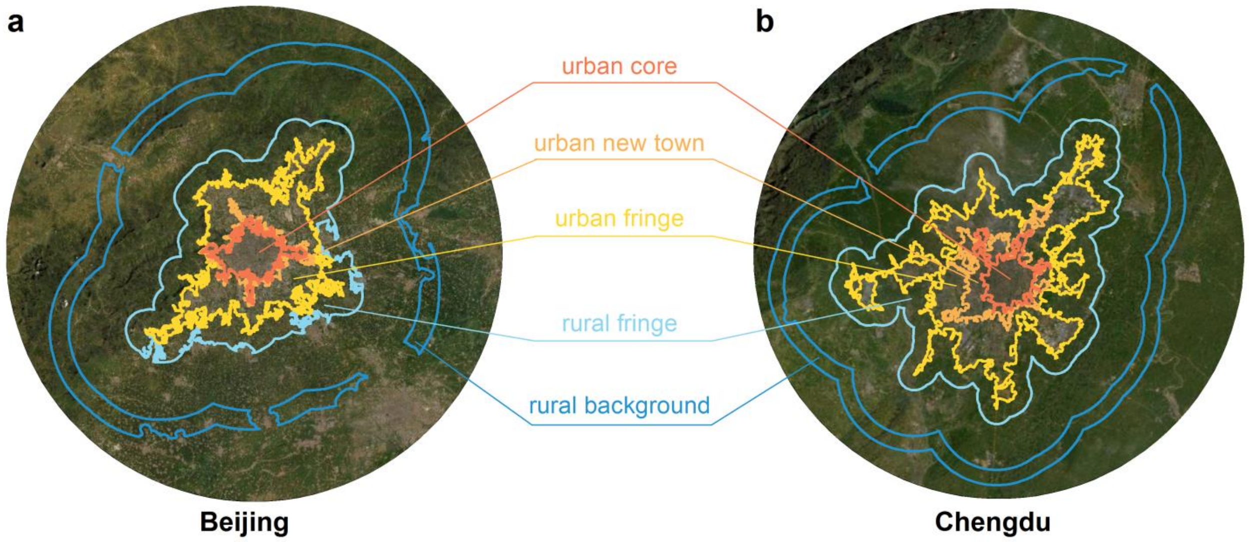

Supplementary Figure 1. Schematic of the three urban and two rural categories for Beijing (a) and Chengdu (b) | Urban cores are delineated by the urban boundaries in 1990, urban new towns include urbanized surfaces from 1990 to 2000, urban fringes include urbanized surfaces from 2000 to 2018, rural fringes are buffer zones around urban fringes with a buffer distance of *d* that guarantees an area of rural fringes equivalent to that of the combination of the three urban categories, and rural backgrounds are delineated by another buffer zone with an area equivalent to the combination of the three urban categories and with a distance of 5*d* from urban fringes for suppressing the impact of urbanization as much as possible (Du et al., 2019).

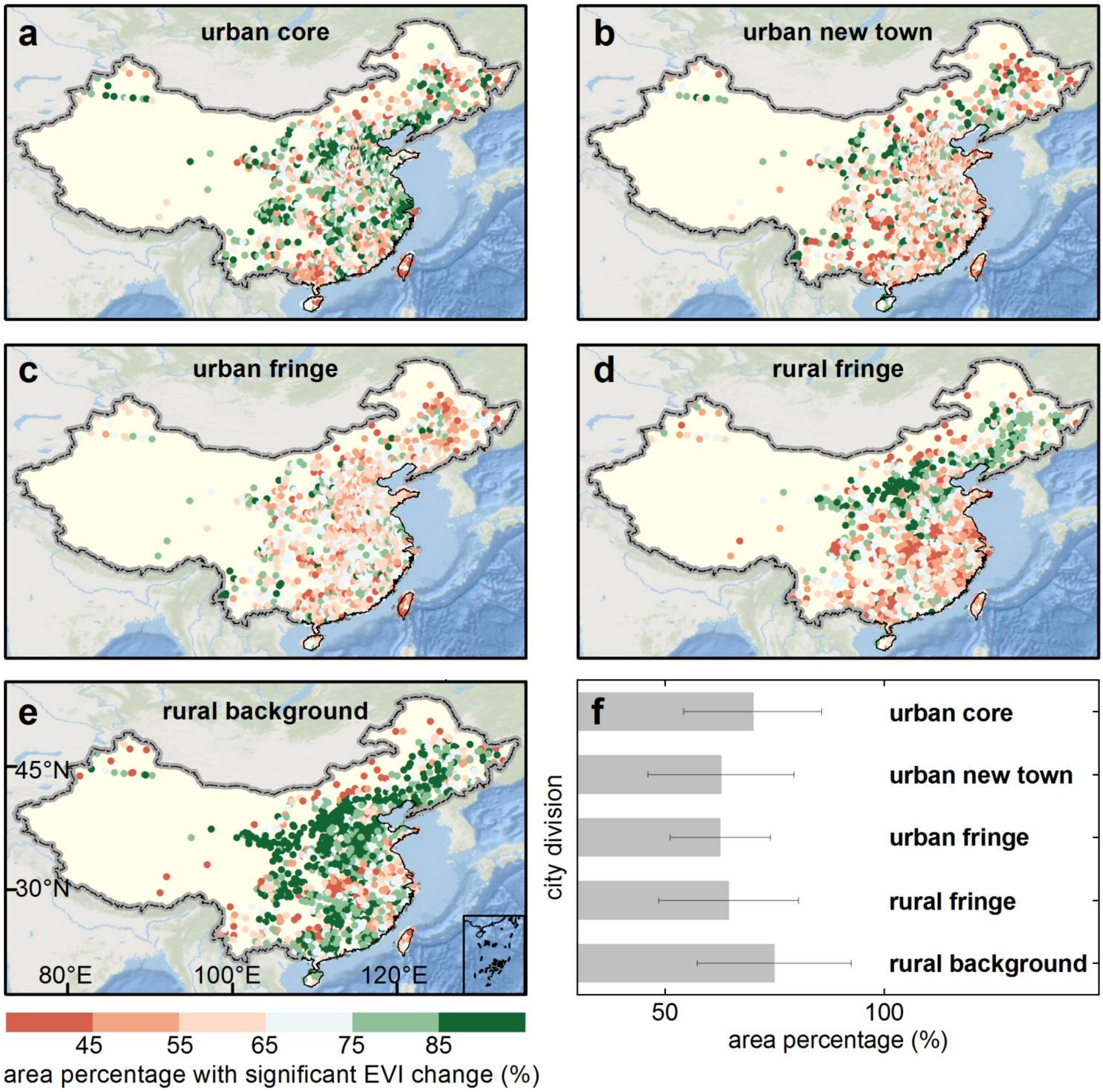

Supplementary Figure 2. Percentage of areas with significant EVI changes (P < 0.05) in the five city categories across 1560 Chinese cities | Area percentages in urban cores (**a**), urban new towns (**b**), urban fringes (**c**), rural fringes (**d**), and **r**ural backgrounds (**e**), and the means and standard deviations in area percentage for the five city categories (**f**).

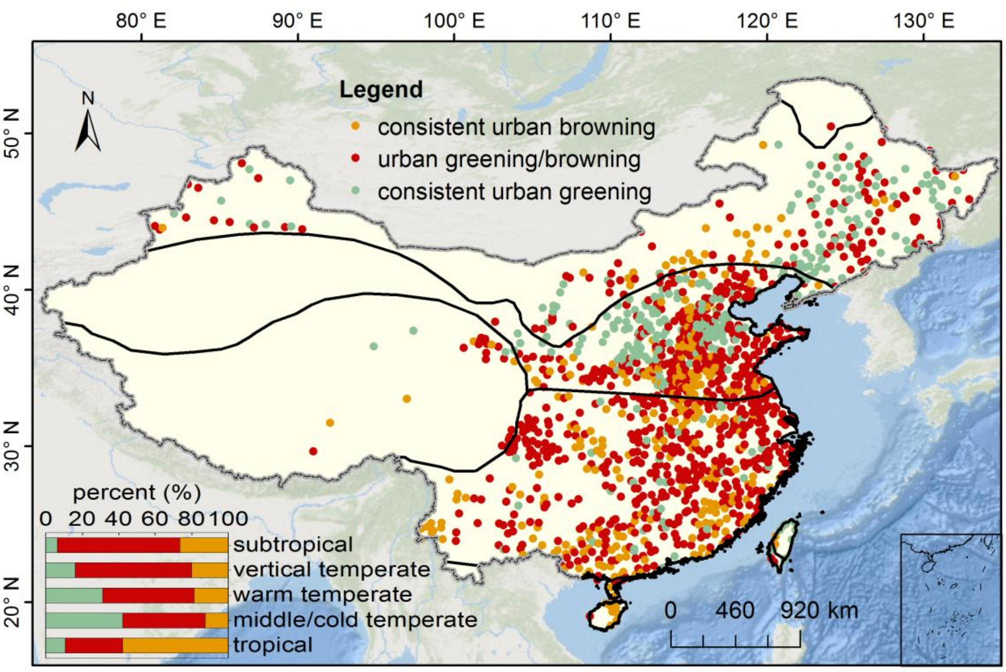

Supplementary Figure 3. Consistency (or heterogeneity) of greenness trends for the three urban categories, urban cores, urban new towns, and urban fringes, and the associated proportions in the climatic zones | Orange indicates that all three urban categories have browning, red indicates that both browning and greening occurs for the three urban categories, and green indicates that all three urban categories have greening.

822

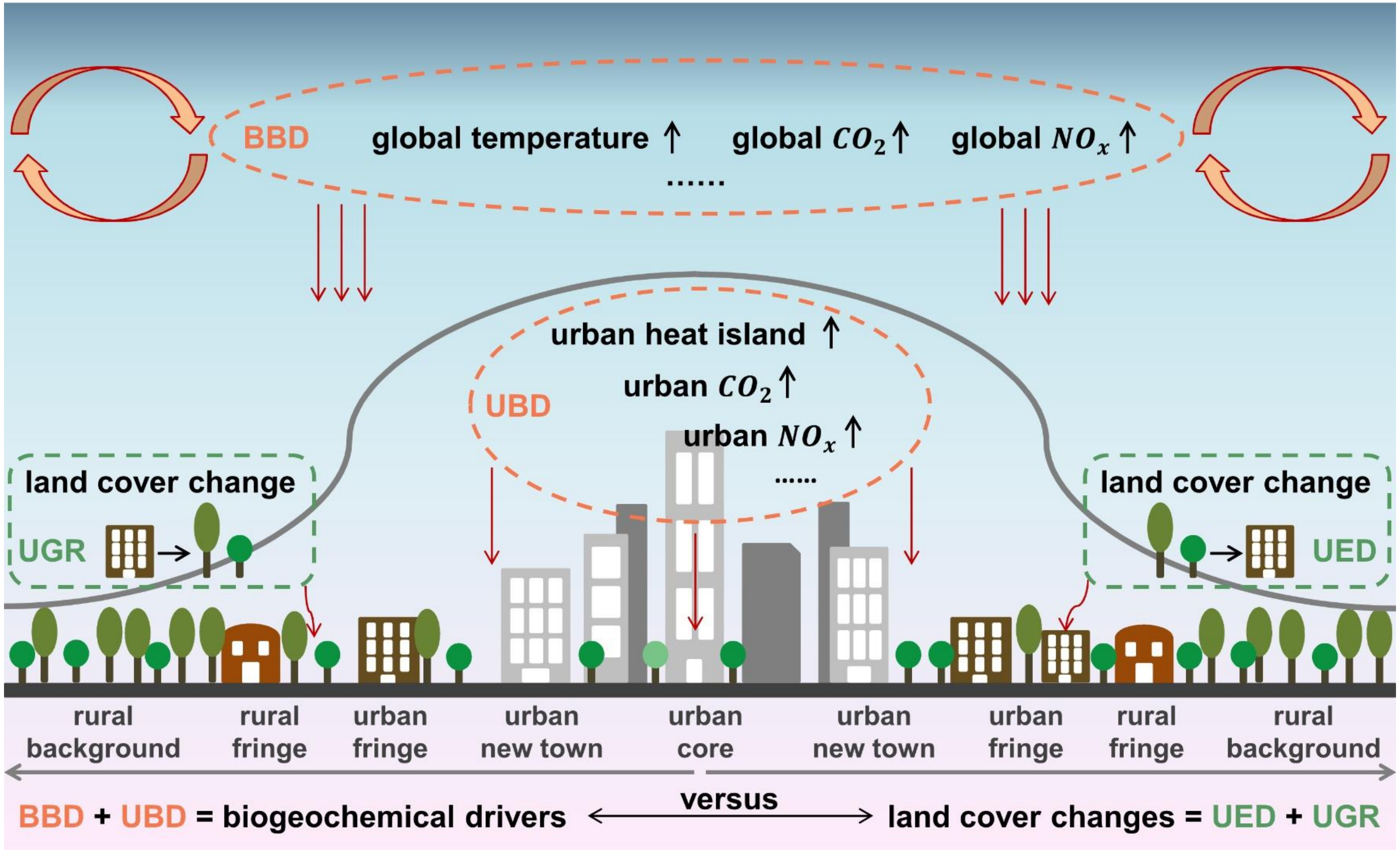

823 **Supplementary Figure 4. Conceptual diagram of the impacts of the background biogeochemical driver (BBD), the urban biogeochemical**

824 **driver (UBD), urban expansion (UED), and green recovery (UGR) on EVI trends** | Biogeochemical drivers include BBD and UBD, and

825 drivers of land-cover changes include UED and UGR.

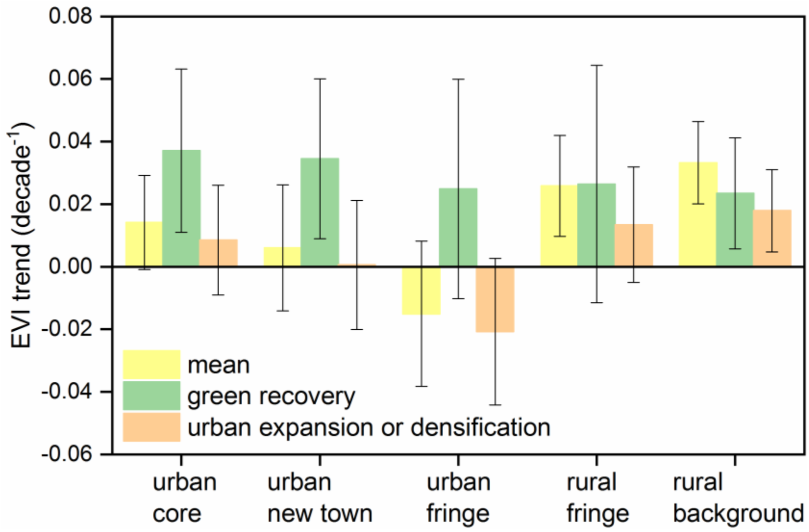

Supplementary Figure 5. Means and standard deviations of the EVI trends for all pixels, the pixels with green recovery, and the pixels with urban expansion or densification for each city category.

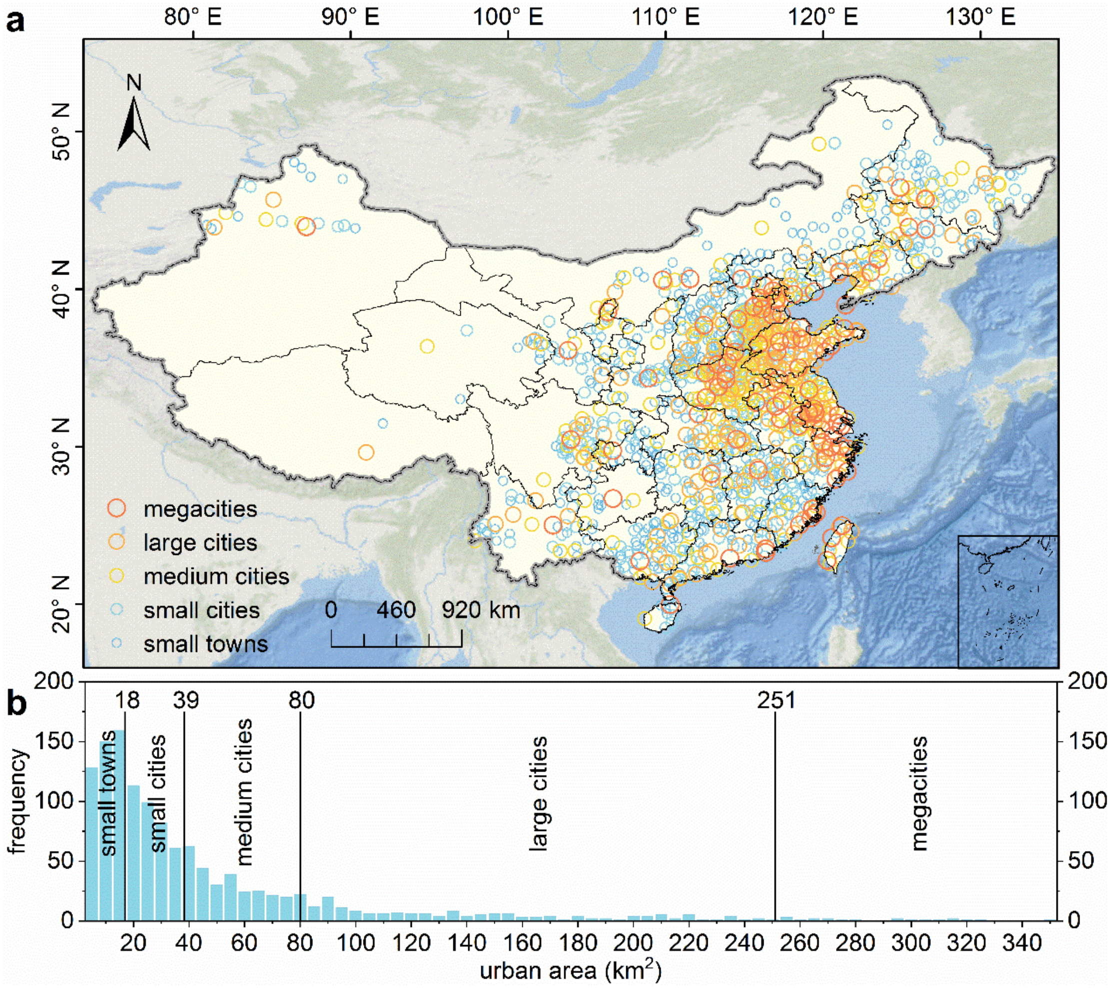

Supplementary Figure 6. Spatial (a) and frequency (b) distribution of city size of the 1560 cities at the county level or above in China | These cities are divided into five categories based on city size: small towns (accounting for 33.3% of all cities), small cities (26.7%), medium-sized cities (20.0%), large cities (13.3%), and megacities (6.7%).

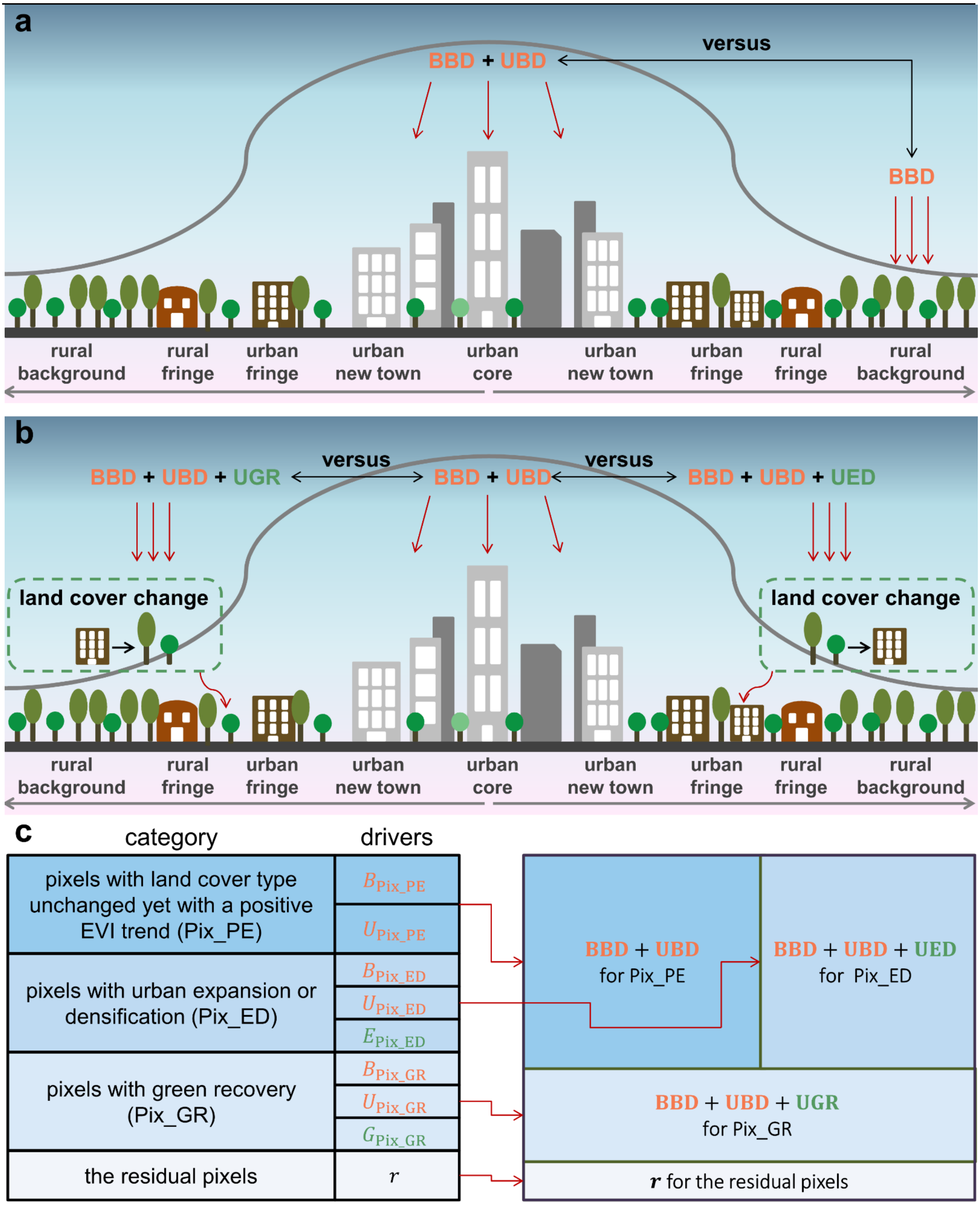

Supplementary Figure 7. Schematic for differentiating between the contribution of each driver for each city category| Comparison of the impacts of the background biogeochemical driver (BBD) and the urban biogeochemical driver (UBD) on the urban-rural gradient of EVI trends (**a**), comparison of the impacts of BBD, UBD, urban expansion or densification (UED), and urban green recovery (UGR) on the urban-rural gradient of EVI trends for areas with and without changes in land-cover type (**b**), and impacts (or contributions) of these four drivers on the EVI trend over different categories of pixels (**c**).

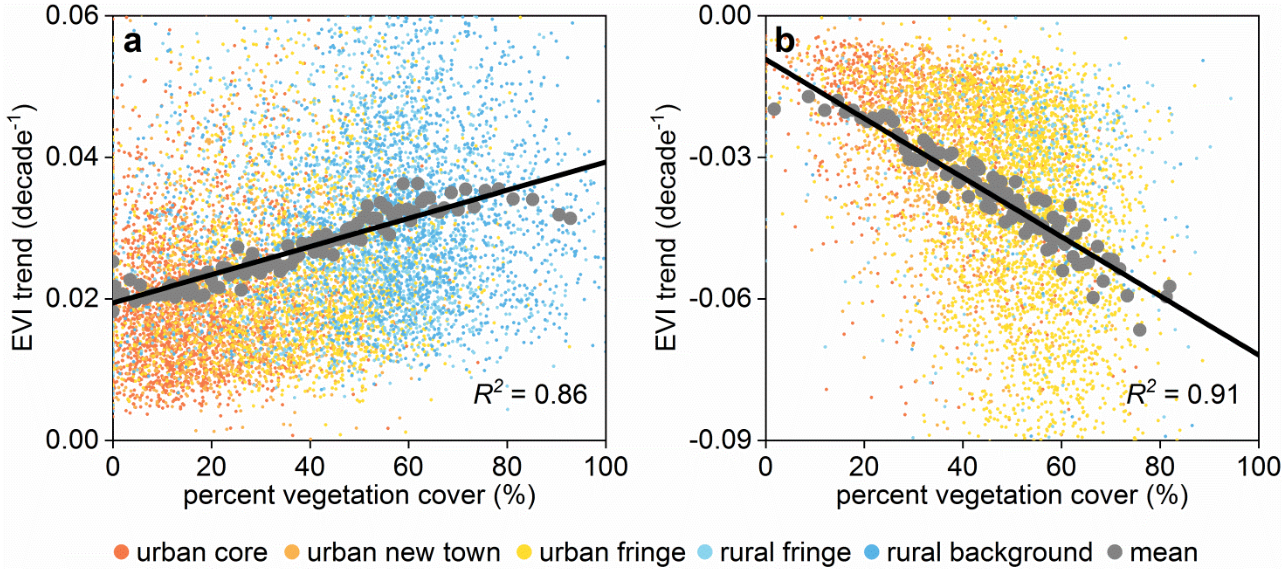

Supplementary Figure 8. Relationship between percent vegetation cover (PVC) and EVI trend | The relationships between PVC and the EVI trends in regions with positive EVI trends (**a**) and regions with negative EVI trends (**b**).

C. Supplementary references

Du, J. et al. Effects of rapid urbanization on vegetation cover in the metropolises of China over the last four decades. *Ecol. Indic.* **107**, 105458 (2019).

Gao, L. et al. Remote sensing algorithms for estimation of fractional vegetation cover using pure vegetation index values: A review. *ISPRS J. Photogramm.* **159**, 364–377 (2020).

Liu, X. et al. Global urban expansion offsets climate-driven increases in terrestrial net primary productivity. *Nat. Commun.* **10**, 1–8 (2019).

Piao, S. et al. Interannual variations of monthly and seasonal normalized difference vegetation index (NDVI) in China from 1982 to 1999. *J. Geophys. Res. Atmos.* **108**, D14 (2003).

Piao, S. et al. Characteristics, drivers and feedbacks of global greening. *Nat. Rev. Earth Environ.* **1**, 1–14 (2020).

Purevdorj, T. S. et al. Relationships between percent vegetation cover and vegetation indices. Int. J. Remote Sens. **19**, 3519–3535 (1998).

Qiu, B. et al. Responses of Australian dryland vegetation to the 2019 heat wave at a subdaily scale. *Geophys. Res. Lett.* **47**, e2019GL086569 (2020).

Tai, X. et al. Plant hydraulic stress explained tree mortality and tree size explained beetle attack in a mixed conifer forest. *J. Geophys. Res. Biogeo.* **124**, 3555–3568 (2019).

Zhang, L. et al. An analysis of shadow effects on spectral vegetation indexes using a ground-based imaging spectrometer. *IEEE Geosci. Remote S.* **12**, 2188–2192 (2015).

Zhao, S. et al. Prevalent vegetation growth enhancement in urban environment. *Proc. Natl. Acad. Sci. USA* **113**, 6313–6318 (2016).

Zhu, Z. et al. Greening of the Earth and its drivers. *Nat. Clim. Change* **6**, 791–795 (2016).